

Microchannel Cooling techniques at LHCb

Oscar Augusto de Aguiar Francisco*

*on behalf of the LHCb VELO Upgrade and CERN PH-DT groups
CERN (CH)*

E-mail: oscar.augusto.de.aguiar.francisco@cern.ch

The thermal management of the LHCb Vertex Detector Upgrade will be provided by evaporative CO₂ circulating in micro-channels or thin tubes. The main plan is to use micro-channels embedded in silicon due to its excellent cooling performance, no thermal expansion coefficient mismatch with electronics and minimal material budget. However, two back-up alternatives are also being investigated: stainless steel tubes embedded in ceramics and titanium 3D printing. The latest prototyping results concerning all cooling substrates alternatives will be described in this proceedings.

*The 26th International Workshop on Vertex Detectors
10-15 September, 2017
Las Caldas, Asturias, Spain*

*Speaker.

1. Introduction

The LHCb Vertex Detector (VELO) will be upgraded in 2018 to a lightweight pixel detector capable of 40 MHz readout to operate at higher luminosity (x5 higher than the current) and very close (5.1 mm) to the LHC beams [1, 2]. Each module is composed of 4 sensors, 12 ASICs and two transceivers (GBTx) that will dissipate around 30 W in the end of the detector lifetime. To minimize the amount of material close to the beam, the electronics (sensor + ASIC) will be overhanging the cooling substrate by 5 mm in innermost region. The sensors should be kept below -20°C to prevent thermal runaway while the expected temperature of the boiling CO_2 will be around -30°C . No leaks can be tolerated since the detector will operate under vacuum. At room temperature, the pressure of the boiling CO_2 is around 65 bar and, according to the CDERN safety regulations, the cooling substrates should be validated up to 186 bar (safety factor of 2.86). Therefore, a new cooling system is necessary due to the new conditions.

Though micro-channel cooling embedded in a silicon plate is gaining considerable attention for applications related to microelectronics, it is still a novel technology for particle physics experiments, in particular when combined with CO_2 evaporative cooling. This technique provides excellent thermal efficiency, no thermal expansion mismatch with silicon ASICs and sensors, radiation hardness of CO_2 , and a very low contribution to the material budget. In parallel to the development of the micro-channel substrate embedded in silicon, the VELO group is also working on the development of two cooling substrate alternatives: capillaries embedded in a ceramic and 3D printed titanium. The latest results concerning all cooling approaches will be described in next sections.

2. Micro-channel embedded in silicon

Micro-channels are composed of two parts: restriction and main channels. The restrictions ($60\ \mu\text{m}$ by $60\ \mu\text{m}$ and 4 cm long) are located before the entrance to a race-track layout of the main cooling channels. They are the dominant pressure drop and ensure even distribution of coolant and prevent flow instabilities among the channels. The sudden increase in cross section between the restrictions and the main channels ($120\ \mu\text{m}$ by $200\ \mu\text{m}$) triggers the boiling of the CO_2 . All channels have almost the same length in total (around 30 cm). Therefore, all channels have similar fluidic resistance. The power dissipation is mainly produced by the six ASIC on front and six located on the back of the substrate (up to 2 W each). Figure 1 shows the design of the micro-channels.

The cooling performance was simulated using the ANSYS software [3]. In this simulation, the power dissipation of 3 W per ASIC was considered (36 W in total) and the attachment to the substrate was simulated as a layer of $100\ \mu\text{m}$ of stycast 8550 FT + catalyst 9 ($1.25\ \text{W}/(\text{m}\cdot\text{K})$). The hottest are is in region overhanging by 5 mm. The maximum variation of temperature is around 5°C when the temperature of the CO_2 is -30°C . A experimental setup that mimics half of a module was also developed as illustrated in the Figure 6. The power dissipation was generated by special heaters designed to simulate the heat pattern in the ASICs and sensors. In total, a power dissipation of 13 W was generated to simulate the end-of-lifetime expectation. This power dissipation corresponds to the expected heat produced by the ASICs ($6 \times 2\ \text{W}$) plus the heat produced by the innermost sensor

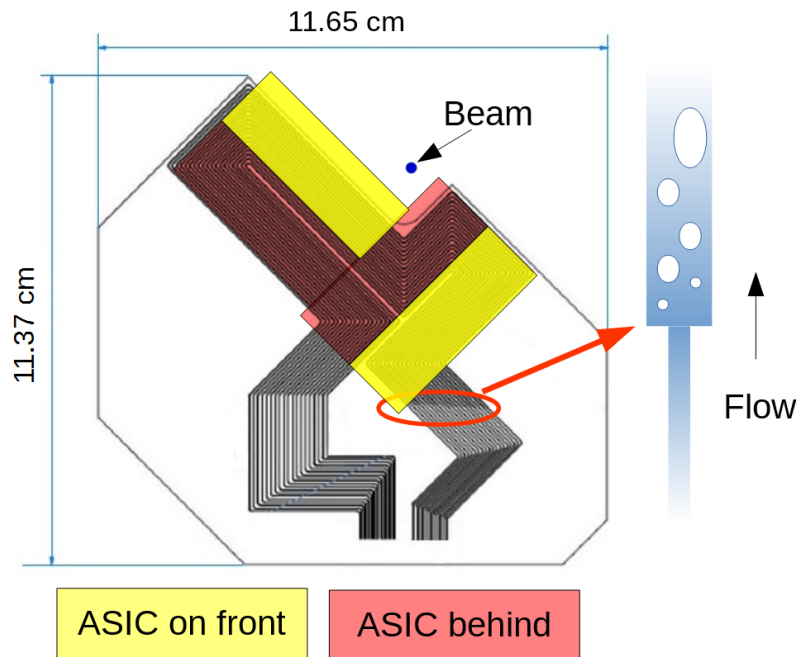


Figure 1: Design of the micro-channels showing the race-track layout and the interface between restrictions and main channels. The heat provided by the electronics is absorbed by the boiling CO_2 in the main channels.

41 (1 W). The power on the outermost sensor is negligible. The maximum variation of temperature in
 42 this conditions is around 6.5°C .

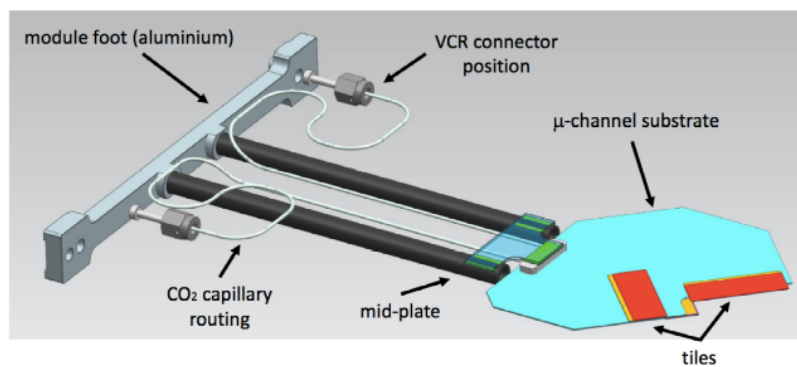


Figure 2: Realistic drawing of the micro-channels substrate with the mechanical support and tiles (sensor + ASICs). The whole substrate is held in place by the midplate glued on the back of the fluidic connector.

43 One of the most challenging stages of the research and development program was the attach-
 44 ment of the fluidic connector to the substrate. The connector is made of invar to minimize the
 45 thermal expansion mismatch and it is attached using a soldering technique. This attachment should
 46 be leak tight since the detector is under vacuum and the module is held by the back side of the
 47 connector, as illustrated in the Figure 2. Therefore, the planarity and parallelism between the con-
 48 nector and the substrate is important for the alignment. On top of that, flux can not be used since
 49 it could corrode the internal parts of the cooling system over the years of operation. The silicon

50 and connector are metalized with layers of titanium (20 nm, silicon only), nickel (0.2-10 μm) and
 51 gold (100 nm) to ensure a good attachment of the solder as illustrated in Figure 3. The soldering
 52 parameters like pressure of the vacuum chamber and temperature cycle were optimized using more
 53 than 150 prototypes before finally achieving a reliable procedure that doesn't introduce significant
 54 stress in the solder joint. On the first soldered micro-channel substrate, a variation of only 11 μm
 55 was found comparing the planarity measurement of the substrate before and after the soldering.
 56 The measurement of the connector height with respect to the silicon surface showed that there is
 57 only a variation of 43 μm , which can be easily absorbed by the glue layer to the support.

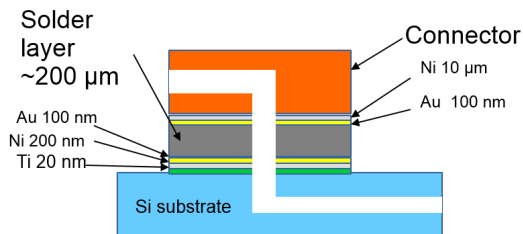


Figure 3: Cross section of the solder joint. The metallization is necessary to ensure a good attachment to both surfaces.

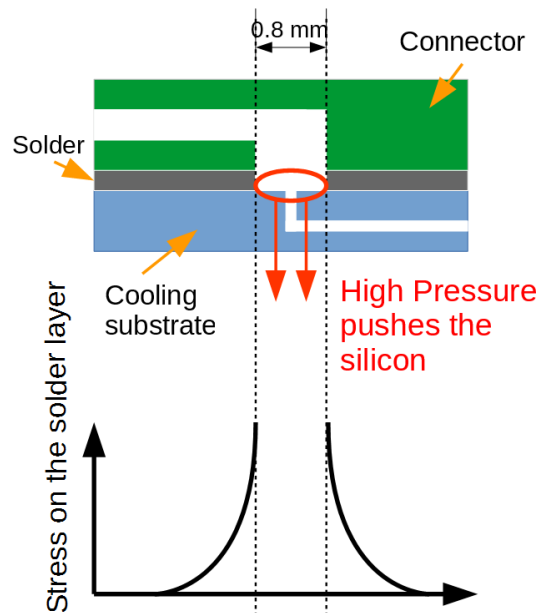


Figure 4: When the system contains high pressure coolant, the region indicated in red is pushed down and the stress is concentrated in the region around the input/output.

58 The solder joint was tested for two long term effects: creep and fatigue. Creep is the plastic
 59 deformation of the material under small mechanical stress levels. This effect is very dependent on
 60 temperature and mechanical load. It becomes relevant typically when the material is warmer than
 61 half of its melting temperature. Usually, it is a very slow effect that might take years or more. In
 62 the other hand, fatigue is the weakening of the material due to a repeatedly applied load. A good
 63 example of this effect are the cracks that appears in asphalt after temperature and pressure cycles.

64 The creep effect was accelerated using a higher mechanical load and temperature than in nom-
 65 inal conditions. Typically, the internal pressure applied was around 60 bar and the samples were
 66 kept at 120 °C. The high pressure is provided by a compressed air bottle and the sample is kept at
 67 high temperature using heaters. A model based on [4] can predict only the behavior of the creep
 68 effect at the linear stage. Based on this model, the acceleration factor using higher temperatures
 69 and loads was obtained. The failure of the material was arbitrary defined as 1% of elongation.
 70 Two cases were considered: even stress distribution over the whole solder joint (case A) or lo-

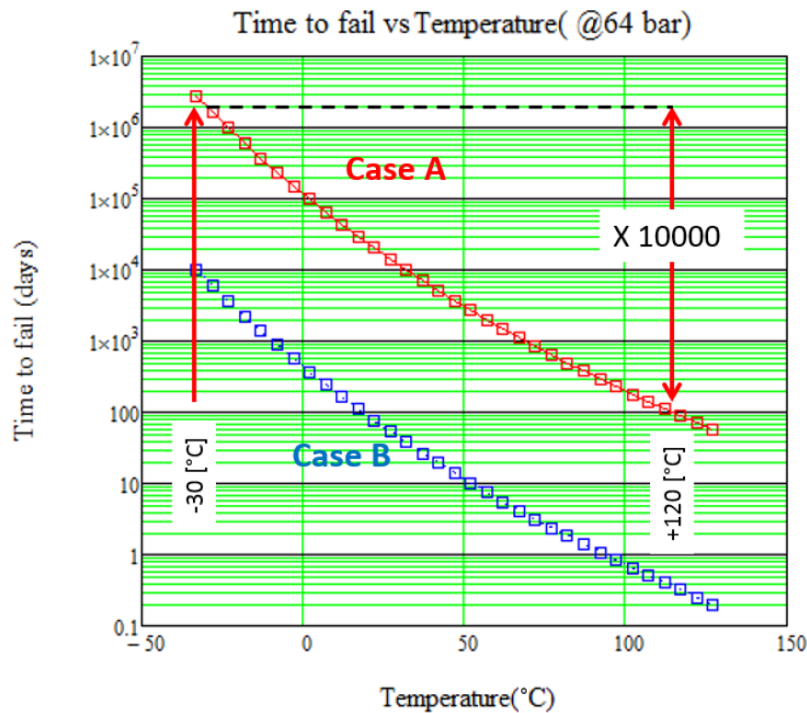


Figure 5: This plot represents the time necessary for the solder layer to elongate by 1% (failure) for a constant pressure of 64 bar as function of the temperature. The case A represents the result obtained when the mechanical stress is uniformly distributed over the whole solder surface and the case B is when the stress is localized on the region close to the input/output. One can notice that comparing the time of failure at $-30\text{ }^{\circ}\text{C}$ and $+120\text{ }^{\circ}\text{C}$, this effect is accelerated by roughly a factor 10000.

71 calized stress around the input/output of the substrate (case B). The case B is more realistic as it
 72 is illustrated in the Figure 4. The results are shown in the Figure 5. Both cases showed similar
 73 acceleration factors of around $\times 10000$ comparing with nominal conditions ($-30\text{ }^{\circ}\text{C}$, 20 bar) and
 74 accelerated conditions ($120\text{ }^{\circ}\text{C}$, 60 bar). This means that 1 hour of accelerated test would corre-
 75 spond to more than 1 year in nominal conditions. In total, 18 samples were tested during 2630
 76 hours (~ 110 days). Only two samples gave in during this test. The first one had a large void close
 77 to one of the slits. Both samples were produced using an experimental technique with a significant
 78 amount of flux. The first sample had a large void close to the slit. In the second sample, there was a
 79 thin layer of flux between the solder and one of the surfaces. Therefore, the usage of flux can also
 80 generate problems in the solder joint it self on the long term. The procedure used to solder the first
 81 micro-channel doesn't use flux.

82 To simulate the fatigue effect, a set-up composed of a chiller and 6 peltiers produces the
 83 temperature cycles from $-40\text{ }^{\circ}\text{C}$ and $+60\text{ }^{\circ}\text{C}$. The high pressure provided by compressed air from
 84 a bottle was used to create pressure cycles from 1 up to 200 bar. In total, 5232 temperature cycles
 85 were performed on 9 samples. For every temperature cycle, 6 pressure cycles were performed.
 86 Only one sample didn't endure the cyclic test. This sample was soldered with an experimental
 87 technique using a significant amount of flux and very fast cooldown rate that could create internal
 88 stress. This sample resisted a single temperature cycle with maximum pressure up to 60 bar and

89 gave in the second temperature cycle with pressure up to 100 bar.

90 Since the cooling system is under vacuum, every couple of cooling loops can be isolated from
 91 the other loops and the cooling plant by two pneumatic valves that will close if any leak is detected.
 92 If too much liquid CO₂ is trapped at cold temperature, this could lead to very high pressures as the
 93 system absorbs heat mostly due to radiation. Therefore, a gas reservoir is necessary in between
 94 the valves in such way that the pressure just follows the saturation curve. This means that at room
 95 temperature the pressure will be around 65 bar. The fluidic characteristics of the final system was
 96 assessed using a dedicated set-up with realistic length of tubes for the input/output, safety valves,
 97 expansion volume and the micro-channels. For the nominal flow of 0.4 g/s, a variation in pressure
 98 of 4.2-5.3 bar was observed for the case where there is no power dissipation and the 30 W case,
 99 respectively. The results are shown in Figure 7.

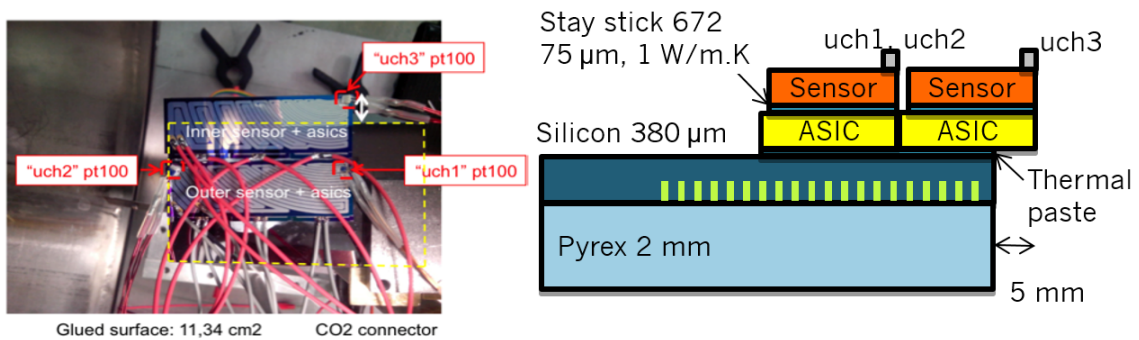


Figure 6: Experimental setup used to evaluate the cooling performance of the micro-channels.

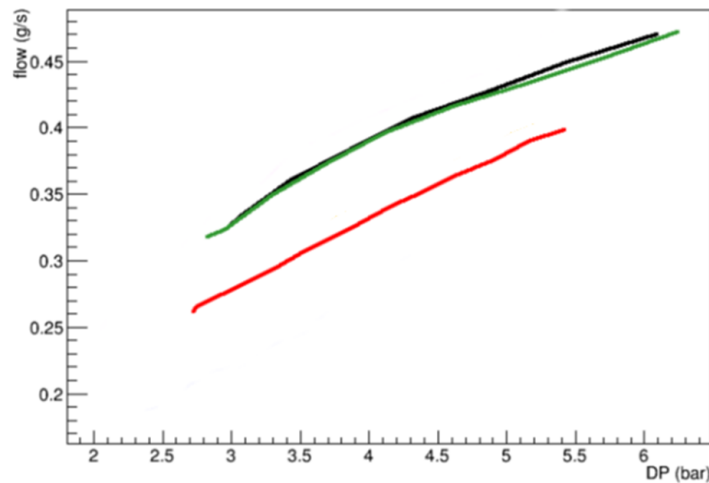


Figure 7: Fluidic characterization of the micro-channels. This plot shows the CO₂ flow through a single micro-channel as function of the pressure difference. The different colors represent the results obtained for 0 W (black), 5 W (green) and 30 W (red). For the nominal flow of 0.4 g/s, a difference in pressure between 4.2 and 5.3 bar is necessary.

100 3. Ceramic substrate

101 One of the cooling substrate alternatives is a more conservative approach composed of a net-
 102 work of four parallel stainless steel capillaries with an outer diameter of 0.8 mm and wall thickness
 103 of 0.3 mm, which are brazed into a manifold. The entrance to the capillary network has 0.16 mm
 104 diameter orifices, which serve as an expansion point and ensures even distribution of the coolant.
 105 Then, the capillaries network is glued into a matching pattern of trenches manufactured inside a 1
 106 mm thick aluminium nitride substrate to serve as mechanical and thermal interface to the electron-
 107 ics. The design is shown in the Figure 8.

108 The thermal performance of a full-scale prototype has been recently tested with one quarter of
 109 the system glued with Stycast: 3 ASIC mockups + 1 sensor mockup (3 x 2W + 1W). A variation of
 110 8 °C was found across the cooling substrate with respect to the temperature of the out going CO₂.

111 Since there are materials with different expansion coefficients (Shapal $4.8 \times 10^{-6}/\text{K}$ and stain-
 112 less steel $16 \times 10^{-6}/\text{K}$), a constraint system is necessary to prevent large deflections of the module
 113 due to temperature variations. The Figure 9 shows the constraint system on the sides of the cooling
 114 substrate. The deflections of the module were under 100 μm .

115 The material simulations have shown that the increase in the average material budget is only
 116 around 6% of the radiation length (χ_0). For the VELO Upgrade a sizeable contribution comes from
 117 the aluminum foil that separates the beam vacuum from the detector vacuum (RF foil). The results
 118 obtained are shown in the Figure 10.

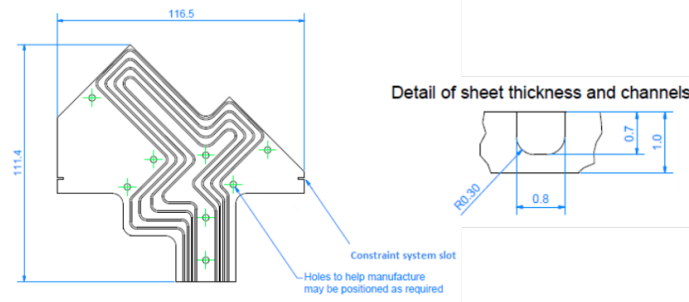


Figure 8: Design of the ceramic substrate. The coolant flows through 4 stainless steel pipes of outer diameter of 0.8 mm and wall thickness of 0.3 mm.

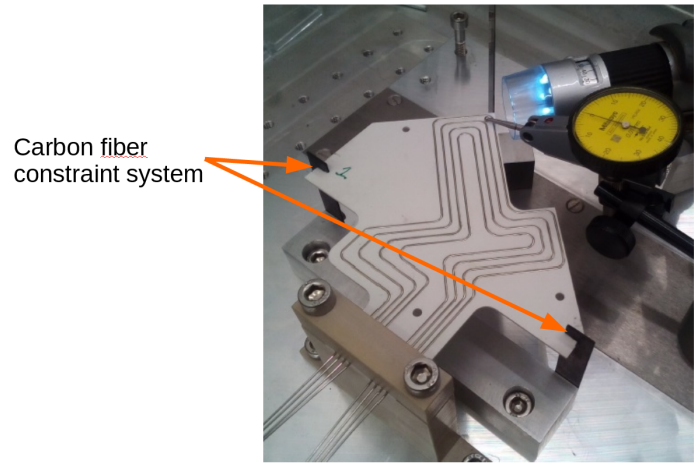


Figure 9: Figure illustrating the constraint system in carbon fiber on the sides of the module.

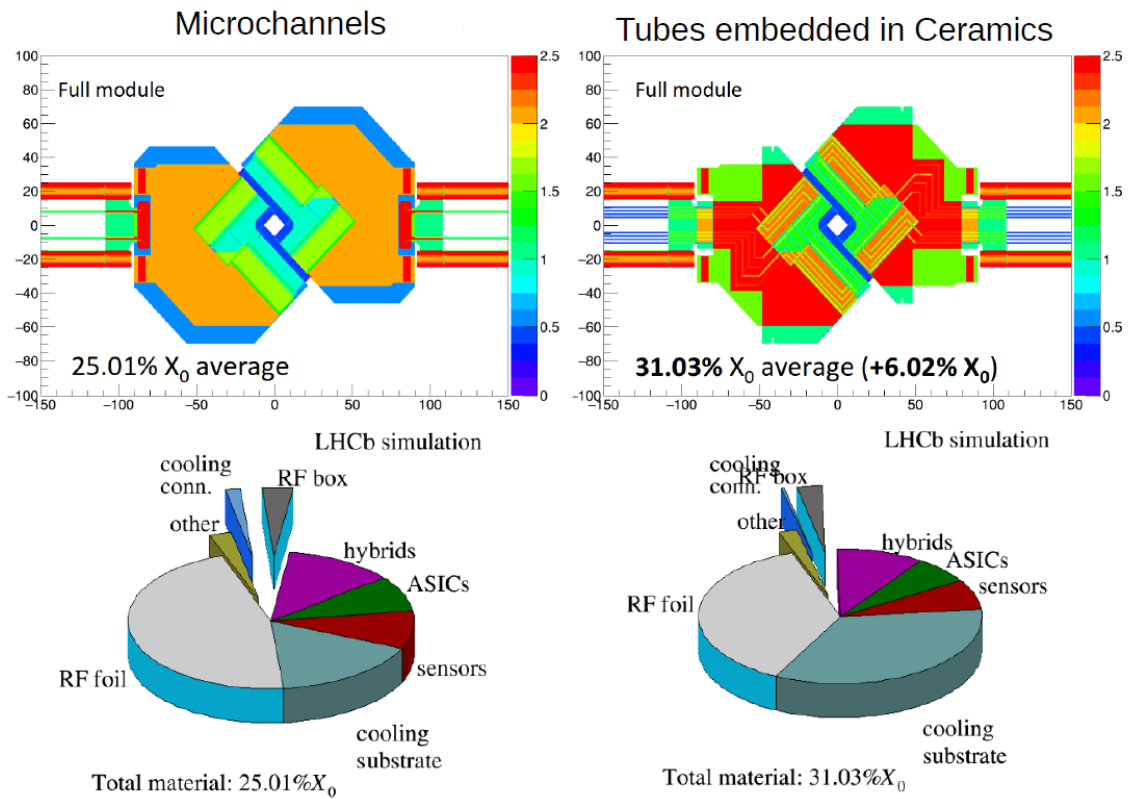


Figure 10: Comparison of the material budget between the micro-channels embedded in silicon (left) and the ceramic substrate (right). A sizeable contribution comes from the RF foil that separates the beam vacuum from the detector vacuum.

POS(Vertex 2017)024

119 4. 3D printing in Titanium

120 The advancements in the 3D printing allow creating structures that would be impossible a
 121 few years ago. Today, a wide variety of material can be used to print 3D objects. The second
 122 substrate alternative is based in 3D printing using titanium. Its powder is fused using a laser beam
 123 to form a 3D object layer by layer. The coolant circulates through four squared titanium tubes
 124 that are just under the electronics like it is shown in the Figures 11 and 12. These substrates are
 125 much faster to produce (quick prototyping). In a single batch that takes a few days, 25 modules
 126 can be manufactured. They are also cheaper than the other cooling substrates previously described
 127 in this document. The restrictions can be integrated in the inlet of the device (0.35 mm x 0.35
 128 mm x 40 mm). It is also easier to handle than the silicon cooling substrate. However, it also
 129 has disadvantages like low thermal conductivity (16 W/(m.K)) and mismatch of thermal expansion
 130 coefficients with respect to the electronics ($6 \times 10^{-6}/K$).

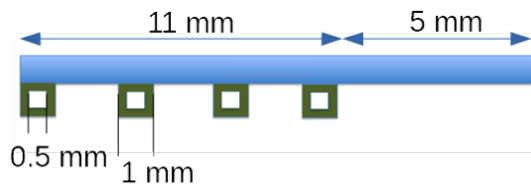


Figure 11: Cross section of the design of the 3D printed substrate. The blue rectangle represents the sensor and ASIC glued on top of the four cooling Ti tubes.

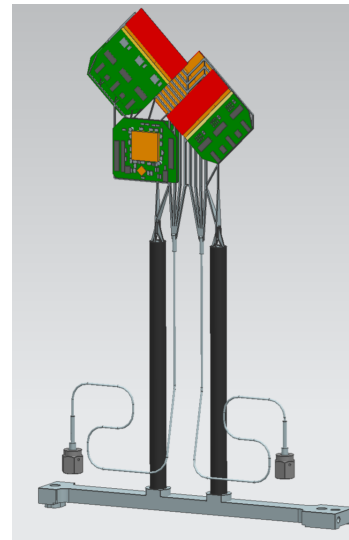


Figure 12: Realistic drawing showing all the electronics components on top of the 3D printed Ti substrate.

131 High pressure tests showed that these structures can withstand up to 250 bar and leak tightness
 132 can be obtained if the walls are at least 250 μm . The deflections due to the temperature variations
 133 are also below 100 μm . There are still many tests to be done to completely validate this alternative.
 134 For instance, due to the limited area for the attachment of the electronics on the cooling substrate
 135 the glue layer should be optimized in such way that it can provide a good attachment and at the same
 136 time minimal variation of temperature. Flatness is also a concern since it is not a solid structure
 137 and the manufacturing reproducibility still has to be proven. On top of that, it should be proven
 138 that there is no detachment of the titanium powder over time.

139 5. Conclusion

140 The micro-channel evaporative cooling has a better physics performance due to the lower
141 material budget. There is no CTE mismatch between the electronics and the substrate since the
142 sensor and ASIC are also made of silicon. No fatigue or accumulated stresses were observed
143 performing long term reliability tests. The first micro-channel substrate was properly attached to
144 the fluidic connector recently.

145 Two back-up alternatives were designed to have similar fluidic characteristics and be easier
146 to handle. The tubes embedded in ceramics is the most conservative approach and it has a good
147 thermal performance but it would required a dedicated constraint system. On the other hand, the
148 3D Titanium printed substrate is evolving quite fast due to the fast prototyping and it is also cheaper
149 than the other alternatives. All technologies are going to be reviewed on late September and the
150 final decision will be taken shortly after.

151 References

- 152 [1] A. A. Alves Jr. et al. The LHCb detector at the LHC. *JINST*, 3:S08005, 2008.
- 153 [2] LHCb Collaboration. LHCb VELO Upgrade Technical Design Report. Technical Report
154 CERN-LHCC-2013-021. LHCb-TDR-013, CERN, Nov 2013.
- 155 [3] ANSYS® Academic Research, Release 14.5, ANSYS, Inc.
- 156 [4] X. Q. Shi, Z. P. Wang, W. Zhou, H. L. J. Pang, and Q. J. Yang. A new creep constitutive model for
157 eutectic solder alloy. *J. Electron. Packag* 124(2), 85-90 (May 02, 2002), 2002.